

# Solution structure of the potassium channel inhibitor agitoxin 2: Caliper for probing channel geometry



ANDRZEJ M. KREZEL,<sup>1,3</sup> CHANDRASEKHAR KASIBHATLA,<sup>1,3</sup> PATRICIA HIDALGO,<sup>2</sup>  
RODERICK MACKINNON,<sup>2</sup> AND GERHARD WAGNER<sup>1</sup>

<sup>1</sup> Department of Biological Chemistry and Molecular Pharmacology, Harvard Medical School, Boston, Massachusetts 02115

<sup>2</sup> Department of Neurobiology, Harvard Medical School, Boston, Massachusetts 02115

(RECEIVED February 28, 1995; ACCEPTED May 17, 1995)

## Abstract

The structure of the potassium channel blocker agitoxin 2 was solved by solution NMR methods. The structure consists of a triple-stranded antiparallel  $\beta$ -sheet and a single helix covering one face of the  $\beta$ -sheet. The cysteine side chains connecting the  $\beta$ -sheet and the helix form the core of the molecule. One edge of the  $\beta$ -sheet and the adjacent face of the helix form the interface with the *Shaker* K<sup>+</sup> channel. The fold of agitoxin is homologous to the previously determined folds of scorpion venom toxins. However, agitoxin 2 differs significantly from the other channel blockers in the specificity of its interactions. This study was thus focused on a precise characterization of the surface residues at the face of the protein interacting with the *Shaker* K<sup>+</sup> channel. The rigid toxin molecule can be used to estimate dimensions of the potassium channel. Surface-exposed residues, Arg<sup>24</sup>, Lys<sup>27</sup>, and Arg<sup>31</sup> of the  $\beta$ -sheet, have been identified from mutagenesis studies as functionally important for blocking the *Shaker* K<sup>+</sup> channel. The sequential and spatial locations of Arg<sup>24</sup> and Arg<sup>31</sup> are not conserved among the homologous toxins. Knowledge on the details of the channel-binding sites of agitoxin 2 formed a basis for site-directed mutagenesis studies of the toxin and the K<sup>+</sup> channel sequences. Observed interactions between mutated toxin and channel are being used to elucidate the channel structure and mechanisms of channel-toxin interactions.

**Keywords:** agitoxin; K<sup>+</sup> channel; NMR; protein; scorpion toxin

Scorpion venoms contain a large number of closely related peptide inhibitors of voltage- and Ca<sup>2+</sup>-dependent K<sup>+</sup> channels. These peptides interact directly with the central catalytic region of K<sup>+</sup> channels—the ion conduction pore. They occlude the pore and prevent ion conduction by binding with one-to-one stoichiometry to the extracellular entryway of the channel (Miller et al., 1985; MacKinnon & Miller, 1988, 1989; Miller, 1988; Giangiacomo et al., 1992). Knowledge of the precise structure and dimensions of scorpion toxins has been most valuable for probing the structure of K<sup>+</sup> channels. The toxin molecules

are used as calipers to measure the dimensions and geometry of the ion conduction pore regions of K<sup>+</sup> channels.

The known scorpion toxin K<sup>+</sup> channel inhibitors are 37–39 amino acids in length and contain six cysteine residues. They fall into three subclasses (Garcia et al., 1994). Within each subclass, toxins show greater than 70% amino acid identity, whereas conservation is less than 50% between members of different subclasses. Sequence alignment with respect to the six cysteine residues also shows that the polypeptide length between the third and fourth cysteines (C3–C4 segment) is not conserved among toxins of different subclasses. In members of the first (ChTx, Lq2, IbTx), second (NxTx, MgTx), and third (AgTx1, AgTx2, AgTx3, KTx) subclass, the segment contains 10, 11, and 9 residues, respectively. These polypeptide length differences occur in a region that is functionally important. The Arg<sup>24</sup> of agitoxins, located within the C3–C4 segment, shows strong electrostatic interaction with Asp<sup>431</sup> on the *Shaker* K<sup>+</sup> channel. In contrast, ChTx and Lq2 interact very weakly with the same Asp residue on the channel.

The NMR structures of ChTx, IbTx, and MgTx are known (Bontems et al., 1992; Johnson & Sugg, 1992; Johnson et al., 1994). The structure of KTx has also been reported recently (Fernandez et al., 1994). The members of the first two subclasses

Reprint requests to: Gerhard Wagner, Department of Biological Chemistry and Molecular Pharmacology, Harvard Medical School, 240 Longwood Avenue, Boston, Massachusetts 02115; e-mail: wagner@wagner.med.harvard.edu.

<sup>3</sup> A.M. Krezel and C. Kasibhatla contributed equally to this work.

**Abbreviations:** AgTx1, AgTx2, AgTx3, agitoxin variants 1, 2, and 3; ChTx, charybdotoxin; Lq2, *Leiurus quinquestriatus* variant 2 toxin; IbTx, iberiotoxin; KTx, kaliotoxin; MgTx, margatoxin; NxTx, noxiustoxin; Stv3, scorpion toxin variant-3; NOESY, NOE spectroscopy; HSQC, heteronuclear single-quantum coherence; TOCSY, total correlation spectroscopy; DQF-COSY, double quantum filtered correlated spectroscopy; 2D, two dimensional; 3D, three dimensional; HNHA and HNHB, <sup>15</sup>N-separated quantitative J-correlation experiments; RMSD, RMS deviation.

have an essentially identical fold consisting of a triple-stranded antiparallel  $\beta$ -sheet linked to an  $\alpha$ -helix by disulfide bridges. The reported structure of KTx shows a different orientation of the first  $\beta$ -strand (Fernandez et al., 1994). This will be further discussed below.

Mutagenesis studies have shown that functionally important residues of ChTx lie on the surface formed by the  $\beta$ -sheet (Stampe et al., 1994). Many of these important residues are not conserved in the subclass 3 toxins even though ChTx and AgTx2 are targeted against many of the same  $K^+$  channels. This observation, as well as the lack of conservation of the length of the C3-C4 segment, motivated us to determine the 3D solution structure of AgTx2 by NMR spectroscopy.

## Results

### Resonance assignments

The  $^1H$  resonances of AgTx2 were assigned with standard homonuclear NMR techniques (Wagner & Wüthrich, 1982; Wüthrich, 1986), using 2D TOCSY (Braunschweiler & Ernst, 1983), DQF-COSY (Piantini et al., 1982; Shaka & Freeman, 1983; Rance et al., 1983), and NOESY (Jeener et al., 1979; Anil-Kumar et al., 1980) spectra. A summary of the sequential connectivities observed is shown in Figure 1. The assignments of backbone amide  $^{15}N$  resonances were obtained from an  $^{15}N-^1H$  HSQC experiment (Bodenhausen & Ruben, 1980). All of the backbone amide  $^{15}N$  and virtually all  $^1H$  resonances were assigned except for the hydroxyl protons of the two threonine and two serine residues. The resonance assignments are listed in Table 1.

Stereospecific proton assignments were accomplished for 19 of 27  $\beta$ -methylene groups (70%). Residues Pro<sup>3</sup>, Asp<sup>20</sup>, Arg<sup>24</sup>, Lys<sup>27</sup>, and Lys<sup>38</sup> had the two signals of the  $\beta$ -methylene groups overlapped at 25 °C, preventing stereospecific assignments. The methyl groups of Val<sup>2</sup> and Val<sup>6</sup> residues were also assigned stereospecifically.

### Conformational constraints

A total of 445 NOE distance constraints were used in the structure calculations. This included 309 interresidue and 136 intraresidue distance constraints. The above numbers do not include intraresidue NOEs that did not constrain the conformation beyond the covalent restraints. Additionally, 26  $\phi$  and 17  $\chi^1$  torsion angle restraints were included in the calculations (Table 2). Two restraints for each of nine hydrogen bonds were used throughout the structure calculations. Disulfide bonds connecting residues Cys<sup>8</sup> to Cys<sup>28</sup>, Cys<sup>14</sup> to Cys<sup>33</sup>, and Cys<sup>18</sup> to Cys<sup>35</sup> were introduced as covalent bonds between S $\gamma$  atoms. They were fully consistent with observed NOEs between  $\beta$ -methylene groups of cysteine residues.

### Secondary structure

The secondary structure of AgTx2 was initially deduced from the pattern of characteristic NOEs between backbone protons ( $H^\alpha$  and  $H^N$ ) and finally established with results of the tertiary structure calculations. NOEs defining the triple-stranded antiparallel  $\beta$ -sheet are shown in Figure 2 (see Kinemage 1). The two outer strands of the  $\beta$ -sheet, S1 and S2, are connected by a helix. The S3 strand, consisting of residues Lys<sup>32</sup>-Thr<sup>36</sup>, is in the center. The N-terminal  $\beta$ -strand S1 (residues Val<sup>2</sup>-Cys<sup>8</sup>) is in-

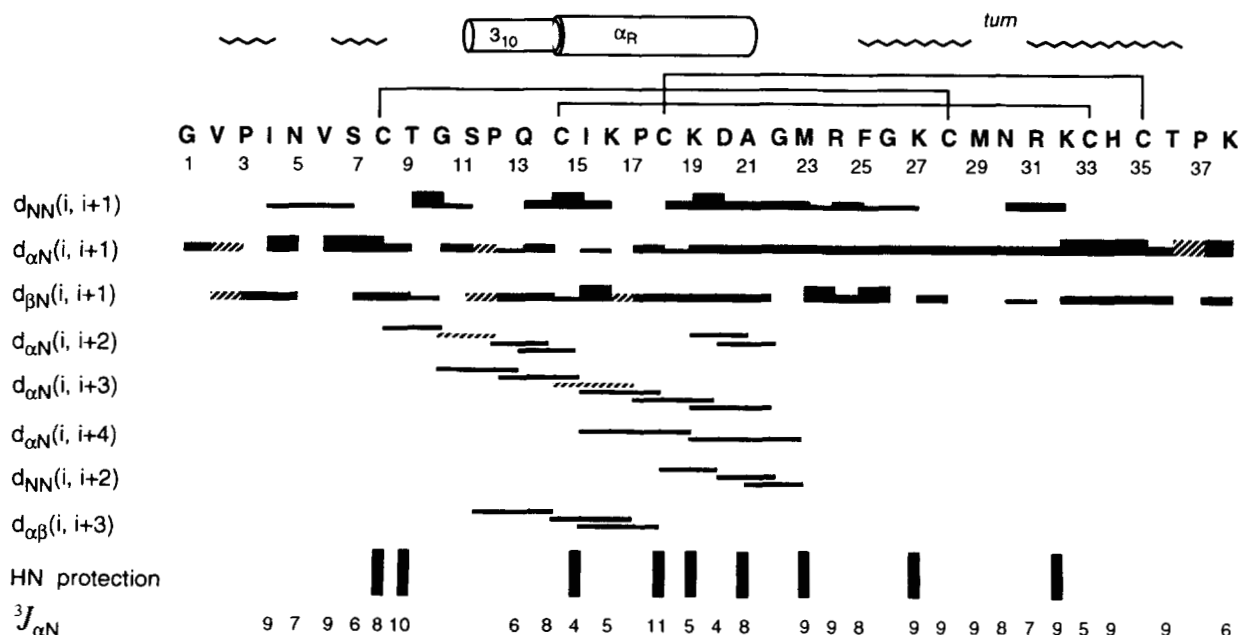


**Fig. 1.** Summary of NOE data used to obtain sequence-specific assignments. Line thickness is proportional to the observed cross peak intensities. Stippled lines correspond to cross peaks involving  $H^\delta$  protons of proline residues. Coupling constants and amide exchange protection factors are also included. Coupling constants were rounded to the nearest integer. The sequence of AgTx2 is shown with lines connecting disulfide-bonded cysteine residues. Secondary structure elements are indicated above the sequence.

**Table 1.** Backbone amide  $^{15}\text{N}$  and  $^1\text{H}$  resonance assignments for AgTx2 at 25 °C and pH 4.5<sup>a</sup>

Residue	N	$\text{H}^\text{N}$	$\text{C}^\alpha\text{H}$	$\text{C}^\beta\text{H}$	$\text{C}^\gamma\text{H}$	$\text{C}^\delta\text{H}/\text{N}^\delta\text{H}$	$\text{C}^\epsilon\text{H}/\text{N}^\epsilon\text{H}$	$\text{C}^\zeta\text{H}$
Gly 1			4.04, 3.88					
Val 2	122.09	9.20	4.62	1.94	0.92, 0.89 <sup>R</sup>			
Pro 3			4.51	1.81, 1.81	2.08, 1.83	3.88, 3.78		
Ile 4	116.72	8.26	4.59	1.89	1.15, 1.02, $\text{C}^\gamma\text{H}_3$ , 0.82	0.66		
Asn 5	122.32	8.74	4.85	2.94, 2.64 <sup>R</sup>		7.64, 6.91 <sup>Z</sup>		
Val 6	122.81	8.00	4.20	1.45	0.99, 0.90 <sup>S</sup>			
Ser 7	123.87	8.65	5.08	3.98, 3.91 <sup>R</sup>				
Cys 8	116.50	7.99	4.95	3.19, 2.95 <sup>S</sup>	2.39, 2.20			
Thr 9	109.85	9.34	4.47	4.39	1.21			
Gly 10	111.19	7.73	4.51, 4.04					
Ser 11	121.09	9.37	4.20	4.15				
Pro 12			4.33	2.46, 1.84 <sup>R</sup>	2.16, 2.01	3.84, 3.63		
Gln 13	113.78	7.34	4.21	2.42, 2.26 <sup>S</sup>	2.57, 2.42		7.65, 6.95 <sup>Z</sup>	
Cys 14	113.89	8.31	4.82	3.10, 2.59 <sup>S</sup>				
Ile 15	123.53	7.21	3.84	1.94	1.67, 1.32, $\text{C}^\gamma\text{H}_3$ , 0.97	0.91		
Lys 16	121.72	9.06	4.30	2.00, 1.85	1.43	1.76, 1.65	3.06	
Pro 17			4.36	2.33, 1.69 <sup>R</sup>	2.37, 2.14	3.66, 3.56		
Cys 18	114.84	7.71	4.47	3.06, 2.39 <sup>R</sup>				
Lys 19	125.16	8.06	4.28	2.04, 1.93	1.59, 1.47	1.71, 1.71	2.98, 2.98	
Asp 20	124.08	9.17	4.39	2.72, 2.72				
Ala 21	121.13	7.38	4.49	1.52				
Gly 22	108.00	8.10	4.18, 3.88					
Met 23	120.46	8.20	4.62	2.14, 1.79 <sup>S</sup>	2.47, 2.33		1.97	
Arg 24	117.08	8.46	4.53	1.37, 1.37	1.19, 1.01	2.84, 2.74	6.83	
Phe 25	115.93	8.25	4.47	3.29, 3.20 <sup>S</sup>		7.23	7.38	7.32
Gly 26	108.50	7.97	4.62, 3.82					
Lys 27	123.95	8.86	4.65	1.73, 1.73	1.35, 1.30	1.66, 1.66	2.93, 2.93	
Cys 28	126.80	8.82	4.93	2.84, 2.48 <sup>S</sup>				
Met 29	130.96	8.94	4.68	1.67, 1.37 <sup>S</sup>	2.20, 2.13		1.83	
Asn 30	126.20	9.42	4.34	3.04, 2.76 <sup>R</sup>		7.67, 6.96 <sup>Z</sup>		
Arg 31	107.60	8.56	4.07	2.33, 2.20 <sup>R</sup>	1.63, 1.63	3.26, 3.26	7.13	
Lys 32	121.09	7.85	5.33	1.97, 1.84 <sup>R</sup>	1.62, 1.55	1.67, 1.67	3.03, 3.03	
Cys 33	122.47	8.56	5.11	2.68, 2.53 <sup>S</sup>				
His 34	122.19	9.53	5.20	3.10, 2.86 <sup>R</sup>		7.17	8.60	
Cys 35	122.08	9.18	5.31	3.13, 2.73 <sup>S</sup>				
Thr 36	119.72	8.80	4.99	4.01	1.47			
Pro 37			4.45	2.37, 2.05 <sup>R</sup>	2.12, 2.02	3.93, 3.93		
Lys 38	126.67	8.32	3.87	1.74, 1.74	1.36, 1.36	1.62, 1.62	2.92, 2.92	

<sup>a</sup> Prochiral atoms are labeled R and S according to the Cahn-Ingold-Prelog rules. The 2 and 3 designations for methylene protons (IUPAC-IUB, 1970) are also indicated with number 2 proton underlined. Side-chain amide protons are labeled with the standard E, Z nomenclature.

**Table 2.** Summary of experimental data used in the structure calculations of AgTx2

Restraint type	Number of constraints
NOE distance constraints (total)	445
Intraresidue	136
Interresidue sequential ( $ i - j  = 1$ )	137
Interresidue medium range ( $2 <  i - j  \leq 4$ )	50
Interresidue long range ( $ i - j  > 4$ )	122
Hydrogen bond distance constraints	$9 \times 2$
Dihedral angle constraints	
$\phi (\text{C}_{(i-1)} - \text{N}_i - \text{C}_i^\alpha - \text{C}_i')$	26
$\chi^1 (\text{N} - \text{C}^\alpha - \text{C}^\beta - \text{X}^\gamma)$	17
Stereospecific assignments	
$\beta$ -Methylene groups	19 of 27 (70%)
$\gamma$ -Methyl groups of valines	2 of 2

interrupted by a  $\beta$ -bulge formed by residues Asn<sup>5</sup> and Val<sup>6</sup>. Strand S2 consists of the residues Arg<sup>24</sup>-Met<sup>29</sup>. The helix starts as a  $3_{10}$ -helix (Ser<sup>11</sup>-Cys<sup>14</sup>) and continues as an  $\alpha$ -helix (residues Ile<sup>15</sup>-Gly<sup>22</sup>). Pro<sup>12</sup> is located in the  $3_{10}$ -helix and Pro<sup>17</sup> in the  $\alpha$ -helix. The reverse turn of type II is formed by residues Met<sup>29</sup>-Lys<sup>32</sup>.

### Tertiary structure

The overall shape of AgTx2 is roughly ellipsoidal, with the long axis about 30 Å and two short axes about 20 Å (see Kinemage 1). The secondary structure elements comprise more than 80% of the sequence of AgTx2. The relative orientation of the secondary structure elements is defined by three disulfide bonds. Two of them (Cys<sup>14</sup> to Cys<sup>33</sup>, Cys<sup>18</sup> to Cys<sup>35</sup>) connect the helix with the central strand (S3) of the  $\beta$ -sheet. The relative positions are

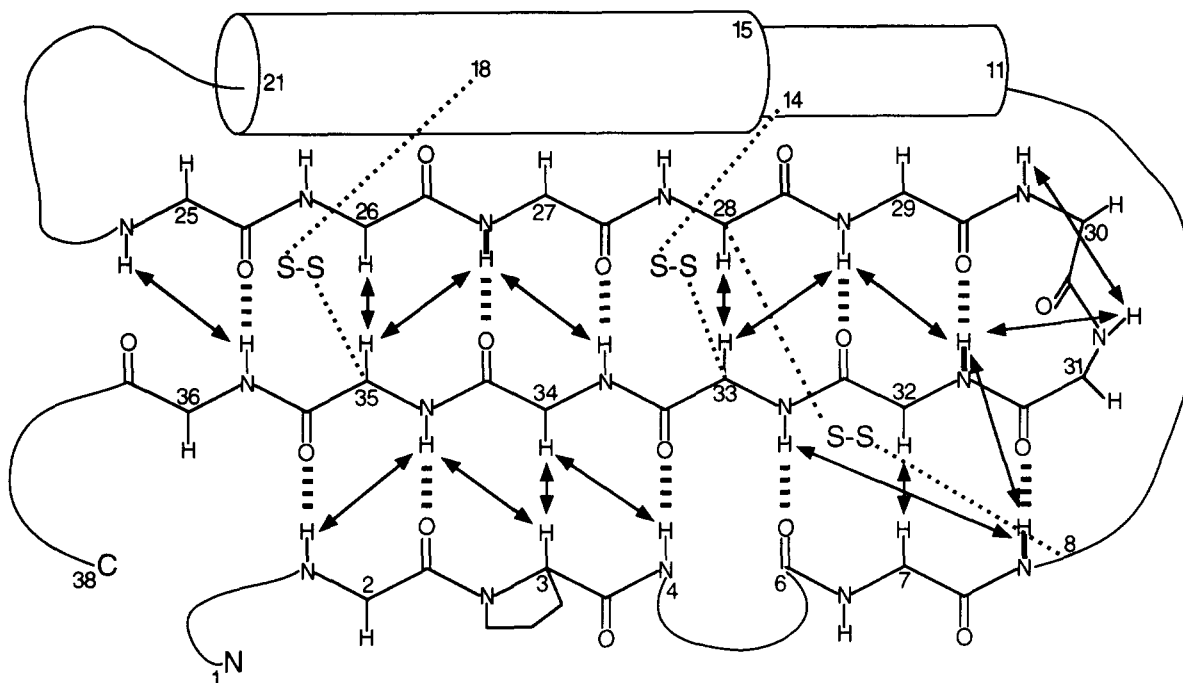


**Fig. 2.** NOEs defining the alignment of the strands in the  $\beta$ -sheet in AgTx2. Strands of the  $\beta$ -sheet are labeled S1, S2, and S3.

additionally fixed by the NOE constraints between residues 14 and 26, 15 and 26, 14 and 33, and 18 and 35 (Fig. 3).

The core of AgTx2 consists of six cysteine residues, Gly<sup>26</sup>, and the side chain of Met<sup>23</sup>. Cysteine residues 14, 33, 18, and 35 are entirely buried, with no solvent-accessible surface area. The backbone atoms of Cys<sup>8</sup> and Cys<sup>28</sup> are partly solvent accessible, 30% and 50%, respectively. Met<sup>23</sup> and Gly<sup>26</sup> are also about 30% accessible. Additionally, Val<sup>2</sup>, Ile<sup>4</sup>, Val<sup>6</sup>, and His<sup>34</sup>

have 50% of their surface in contact with solvent. The most solvent-exposed residues (above 90%) are: 1, 3, 5, 7, 9, 12, 21, 27, 29, 30, 37.

The hydrogen bonds identified in the structure are listed in Table 3. Hydrogen bonds used as restraints in the structure calculations are indicated with double-headed arrows. The 3<sub>10</sub>-helix shows three hydrogen bonds. The hydrogen bonding pattern of the helix is interrupted by the side chain of Pro<sup>12</sup>. The  $\alpha$ -helix shows five regular hydrogen bonds. The amide proton of Gly<sup>22</sup> and Met<sup>23</sup> are within the hydrogen bonding distance from the carbonyl oxygen of Cys<sup>18</sup>. Other potential hydrogen bonds found in the final ensemble of structures are also listed in Table 3.

#### Quality of structure

With 509 conformational constraints (NOEs, dihedral angles, hydrogen bonds, disulfide bonds) and 38 residues, the structure of AgTx2 is very well defined (Table 2; Fig. 4). The RMSDs of atomic coordinates for 17 structures reported here are summarized in Table 4 (see Kinemage 1). The average backbone RMSD of residues 3–36 is 0.37 Å (Fig. 5E). Only the first and last two residues show slightly increased RMSDs. The side chains of most residues are also well defined, with the exception of all five lysine residues, Asp<sup>20</sup>, Met<sup>29</sup>, and Arg<sup>31</sup>. The side chain of Arg<sup>24</sup> is defined better than other charged residues.

The angular order parameters (Hyberts et al., 1992) for the backbone torsion angles of 17 AgTx2 structures are almost all above 95%. The exceptions are the N- and C-termini and residues 9 and 10. The  $\psi$  torsion angle of Thr<sup>9</sup> and  $\phi$  angle of Gly<sup>10</sup> show an angular order parameter of 66%. The average angles are consistent with the observed secondary structure elements. The  $\chi^1$  angles and order parameters are also shown in Figure 5C

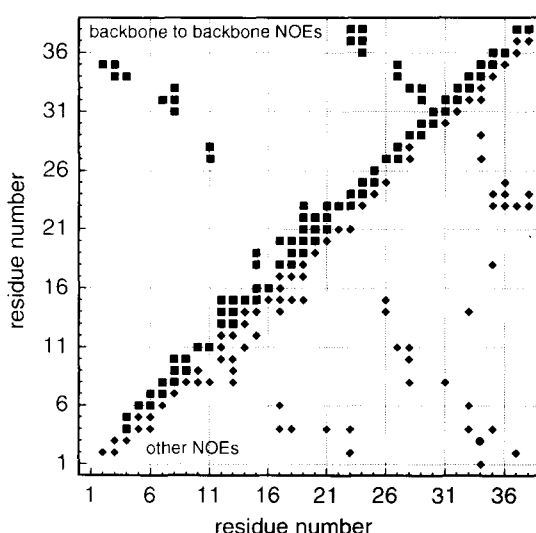


**Fig. 3.** Residue contact map based on the observed NOE cross peaks for AgTx2. Above the diagonal half shows the backbone-backbone contacts involving only H $\alpha$  and H $\beta$  atoms. Below the diagonal half show all remaining contacts.

**Table 3.** Hydrogen bonds of the AgTx2 structure<sup>a</sup>

Acceptor, donor	Acceptor, donor	Average	
		Distance (Å)	Angle (°)
<b>Hydrogen bonds between S1 and S3 strands of the <math>\beta</math>-sheet</b>			
V2 NH	OC C35	2.55	132
V2 CO	HN C35	2.31	120
I4 NH	OC C33	2.36	153
V6 CO	HN C33	2.42	165
C8 NH	↔ OC R31	2.31	107
<b>Hydrogen bonds between S2 and S3 strands of the <math>\beta</math>-sheet</b>			
R24 NH	OC T36	2.03	164
F25 NH	OC T36	2.75	140
F25 CO	↔ HN T36	2.19	135
K27 NH	↔ OC H34	2.31	135
K27 CO	↔ HN H34	2.32	169
M29 NH	↔ OC K32	2.15	131
M29 CO	↔ HN K32	2.31	122
<b>Hydrogen bonds in <math>3_{10}</math>-helix</b>			
G10 CO	HN Q13	2.87	139
S11 CO	HN C14	2.60	143
P12 CO	HN I15	2.62	135
<b>Hydrogen bonds in <math>\alpha</math>-helix</b>			
C14 CO	↔ HN C18	2.19	172
I15 CO	↔ HN K19	2.22	166
K16 CO	HN D20	2.04	174
P17 CO	↔ HN A21	2.31	166
C18 CO	HN G22	2.18	168
C18 CO	HN M23	2.32	130
<b>Other hydrogen bonds</b>			
S11 C <sup>3</sup> O	HN C28	3.09	116
R24 N <sup>6</sup> H	OC P37	3.06	118

<sup>a</sup> Hydrogen bond constraints used in the structure calculations are indicated as double-headed arrows. They were defined as H<sup>N</sup> to O' distance lower and upper limit of 1.80 and 2.30 Å and N to O' distance lower and upper limit of 2.50 and 3.30 Å.

and D, respectively. The  $\chi^1$  order parameters for Arg<sup>31</sup> and Lys<sup>32</sup> are above 95% even though the RMSDs for all of their side-chain atoms combined are rather large (Fig. 5E). The  $\chi^2$ ,  $\chi^3$ , ... order parameters for these residues are around 50%.

The only positive value of  $\phi$  for a non-glycine residue was observed for Arg<sup>31</sup>. This residue is in the  $i + 3$  position of the type II reverse turn. The average  $\phi_{30}$ ,  $\psi_{30}$  ( $i + 2$  position),  $\phi_{31}$ , and  $\psi_{31}$  ( $i + 3$  position) for this turn are: -62°, 101°, 66°, and 6°, respectively. Overall, 79.3% backbone torsion angles of AgTx2 structures fall into the most favorable region of the Ramachandran plot (Ramachandran et al., 1963; Laskowski et al., 1993). The remaining 20.7% backbone torsion angles fall into the additional allowed regions (Laskowski et al., 1993) (Fig. 6).

The average disulfide bond angles { $\chi^2$ ,  $\chi^3$ ,  $\chi^{2'}$ } for Cys<sup>8</sup>-Cys<sup>28</sup> were {164°, 91°, 152°}, for Cys<sup>14</sup>-Cys<sup>33</sup> {-77°, -82°, -56°}, and for Cys<sup>18</sup>-Cys<sup>35</sup> (15 of the 17 structures) {-59°, -79°, -60°}. The standard deviations of those angles were smaller than 7°. Two of the structures showed positive  $\chi^3$  for Cys<sup>18</sup>-Cys<sup>35</sup> disulfide bond with angles with { $\chi^2$ ,  $\chi^3$ ,  $\chi^{2'}$ } = {-167°, 73°, -178°}.

The residual violations of the distance restraints in the presented structures are small and do not show any consistent maxima (Fig. 5B). The average numbers of violations per structure were: 35.5 for violations  $\leq 0.1$  Å; 2.8 for violations between 0.1 Å and 0.2 Å; and 0.5 for violations between 0.2 Å and 0.3 Å. The largest violation in any structure was 0.25 Å. There were no violations of torsion angle restraints larger than 2°.

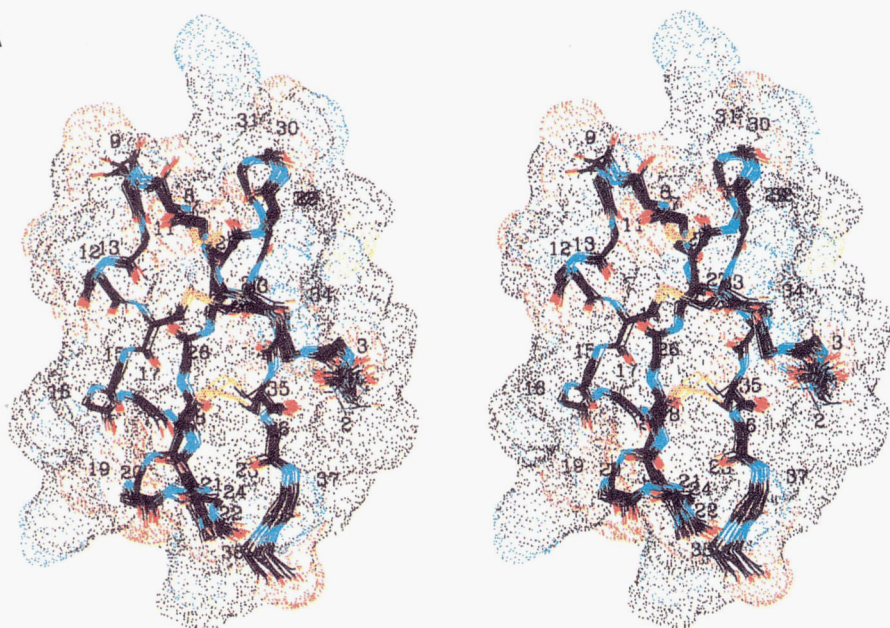
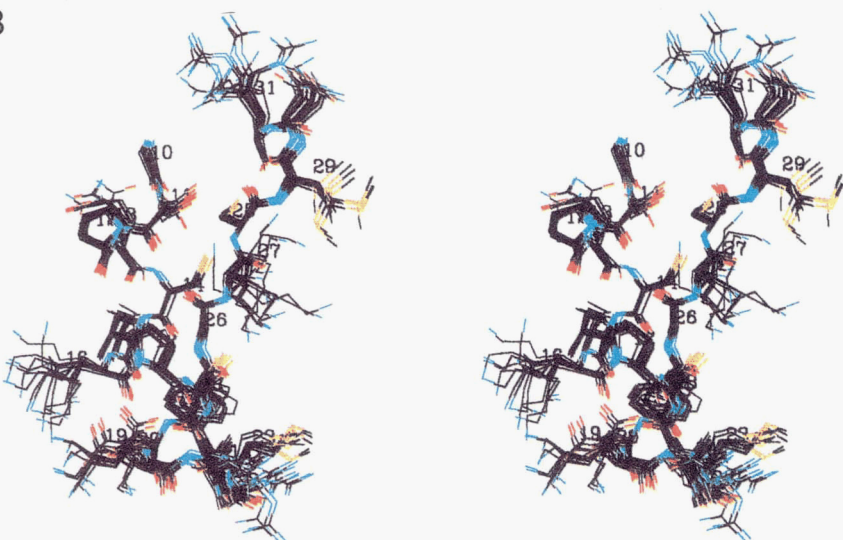
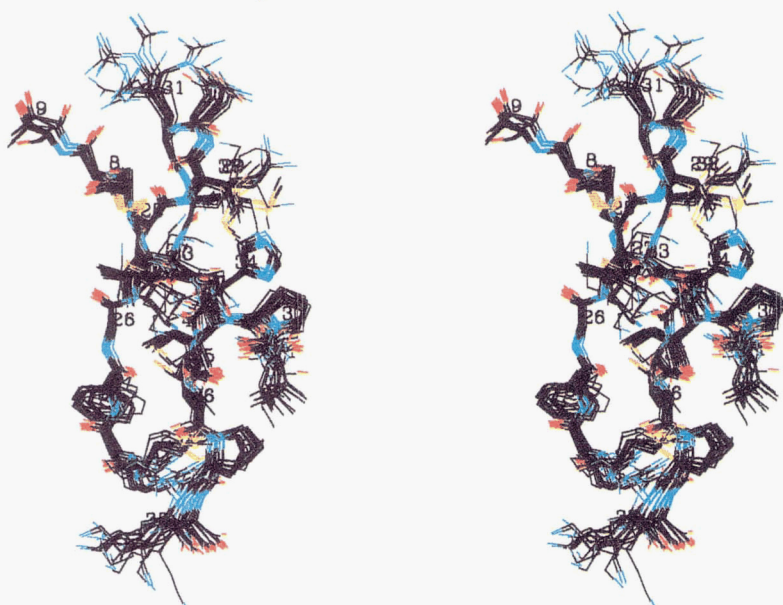
## Discussion

Agitoxin 2 shares the pattern of disulfide bonds and the secondary structure elements with the large and still growing family of proteins isolated from arthropods. So far, there are two distinct subfamilies within this family, scorpion toxins and insect defensins (Bontems et al., 1991a). Members of each subfamily are involved in different processes and possess different functions. The size of proteins within each subfamily varies between 30 and 70 residues. In the last 2 years, the refined X-ray structure of the 65-residue Stv3 (Zhao et al., 1992) and the solution structure of the 31-residue P05-NH<sub>2</sub> scorpion toxin analogue (Muenier et al., 1993) became available. The 3D superposition of these structures, along with ChTx and AgTx2, is shown in Figure 7 (see also Fig. 3 in Bontems et al., 1991b). The secondary structure elements take up about 75% of the sequence of these small proteins and are additionally stabilized by three disulfide bonds forming the core of the molecule. The relative orientation of the hairpin (strands S2 and S3) and the helix is very well conserved. The bulge observed in the first strand of the  $\beta$ -sheet in AgTx2 is also well preserved in other toxin structures.

**Table 4.** RMSDs of atomic coordinates of 17 AgTx2 structures<sup>a</sup>

	Superimposed residues					
	1-38		2-37		3-36	
	Pairwise	To the mean	Pairwise	To the mean	Pairwise	To the mean
<b>Superimposed atoms</b>						
N, C <sup>α</sup> , C'	0.48 ± 0.11	0.33 ± 0.08	0.40 ± 0.11	0.28 ± 0.08	0.37 ± 0.11	0.25 ± 0.08
N, C <sup>α</sup> , C', O'	0.56 ± 0.13	0.38 ± 0.09	0.45 ± 0.13	0.33 ± 0.09	0.42 ± 0.13	0.29 ± 0.09
Heavy atoms	1.25 ± 0.15	0.86 ± 0.11	1.18 ± 0.15	0.81 ± 0.11	1.18 ± 0.16	0.81 ± 0.11

<sup>a</sup> The average values ± standard deviations are given.

**A****B****C**

**Fig. 4.** **A:** Stereo diagram showing 17 calculated structures of AgTx2. All backbone heavy atoms and the disulfides are shown; black, carbon; blue, nitrogen; red, oxygen; yellow, sulfur. A dotted solvent-accessible surface area is shown for one of the structures. **B:** Residues 10-31 (helix and strand S2) with all heavy atoms. This part of the molecule has been shown to interact directly with the channel. **C:** Residues 1-9 and 23-38 forming the triple-stranded antiparallel β-sheet. **D:** Ribbon diagram (Kraulis, 1991) of the structural model with the lowest residual violations of restraints. **E:** Stereo diagram showing the same structure as in part D with all residues labeled. (*Continues on facing page.*)

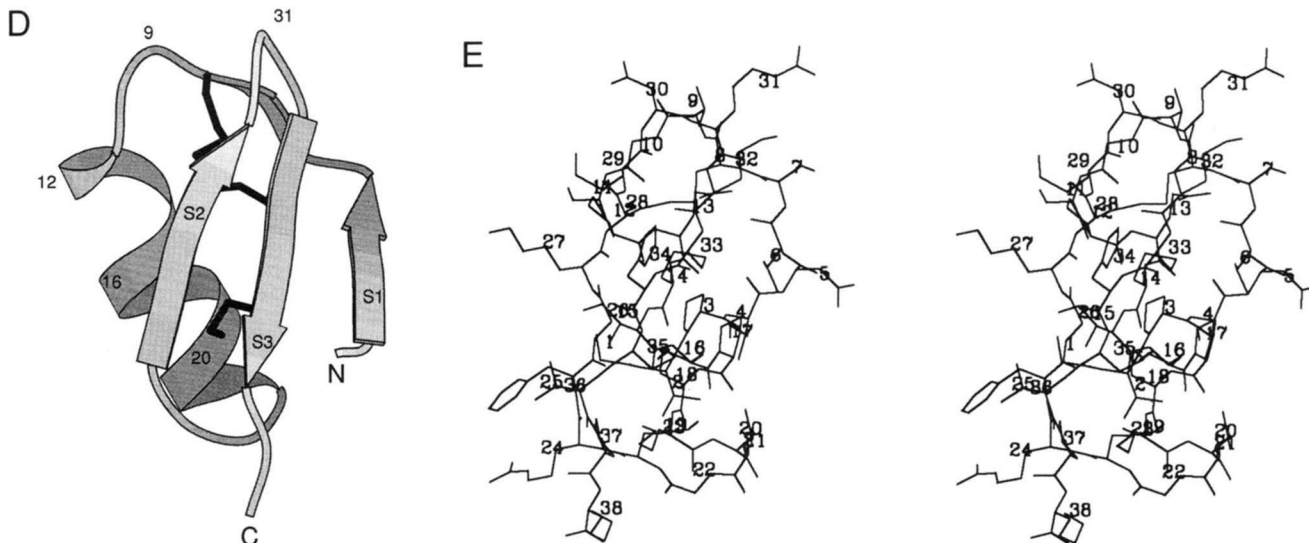
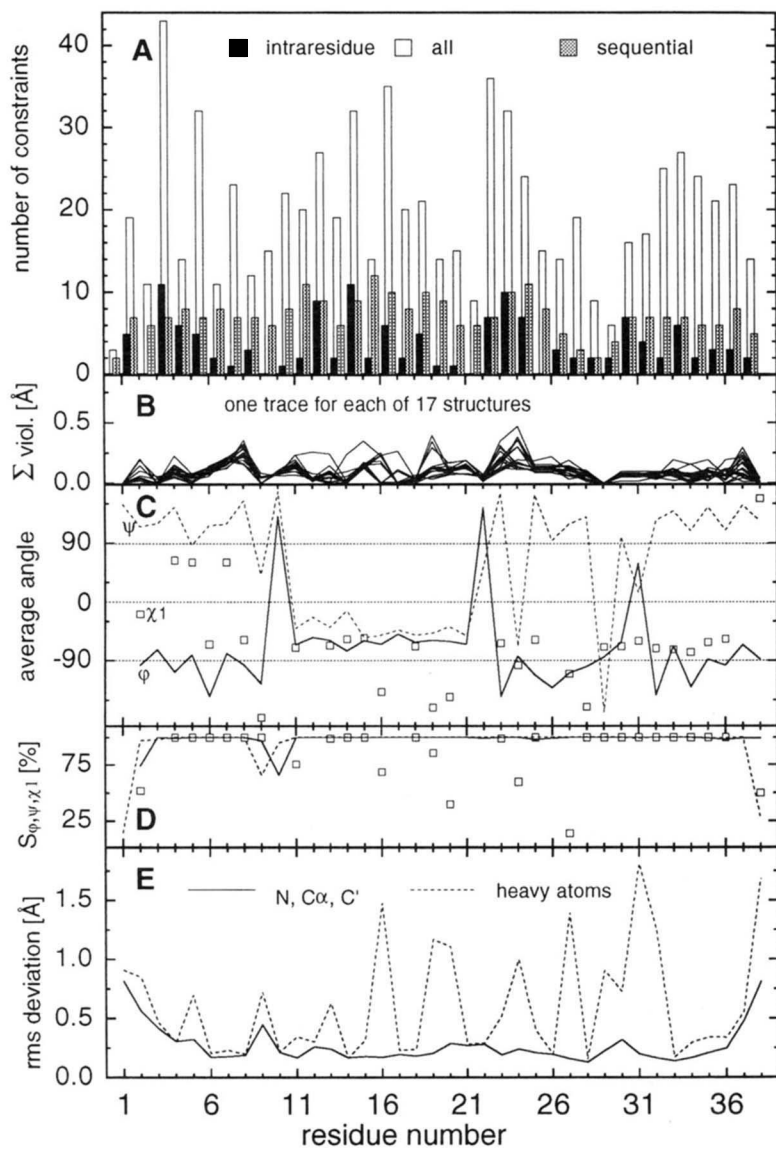
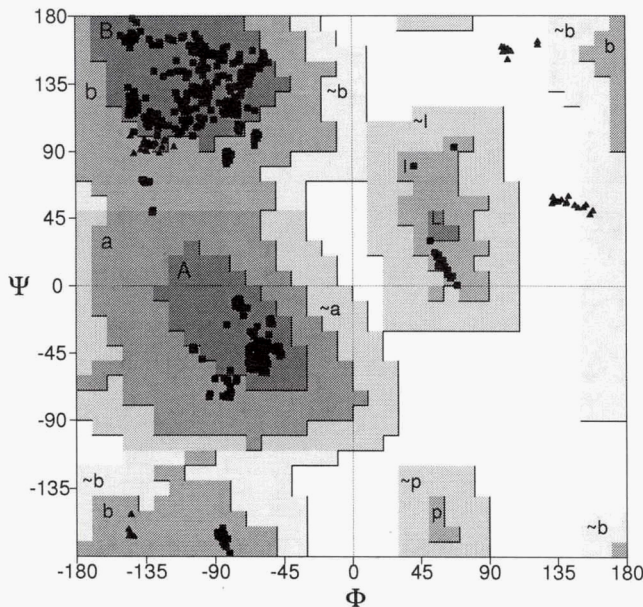


Fig. 4. Continued.



**Fig. 5.** **A:** Number of distance constraints derived from observed NOE cross peaks. Intraresidue, sequential, and all NOE constraints combined for each residue are shown. **B:** Sum of violations for each residue in 17 structures. **C:** Average values of  $\phi$  (solid line),  $\psi$  (broken line), and  $\chi^1$  (open squares) torsion angles for each residue in 17 structures. **D:** Angular order parameters for  $\phi$  (solid line),  $\psi$  (broken line), and  $\chi^1$  (open squares) torsion angles. **E:** Average RMSDs of coordinates for N, C $\alpha$ , C' atoms (solid line), and all heavy atoms (broken line) for each residue in 17 structures. Structures were superimposed on backbone atoms of residues 3–36 of the average structure.



**Fig. 6.** Ramachandran plot of  $\phi$  and  $\psi$  torsion angles for 17 structures calculated for AgTx2. Plot statistics from PROCHECK (Laskowski et al., 1993): residues in most favored regions (A, B, L), 79.3%; residues in additional allowed regions (a, b, l, p), 20.7%. Glycines are shown as triangles. Prolines and end residues are not shown.

Stv3 has a short hairpin budding out in this position. The sequence alignment shown in Figure 8 was based on the spatial correspondence of the polypeptide backbone of amino acid residues.

The Gly<sup>26</sup> position of AgTx2 corresponds to the glycine residue in all known structures of scorpion toxins and insect defensins (Bontems et al., 1991b; Bonmatin et al., 1992). Any other residue in this position would disturb packing of the helix-sheet interface. The side chain of Met<sup>23</sup> occupies the position filled by hydrophobic side chains in other scorpion toxins, although the backbone position of those residues is not conserved. The hydrophobic interactions of the side chain of Met<sup>23</sup> with

the side chain of Cys<sup>18</sup> are also consistent with the Schellman motif in the helix C-terminal cap (Aurora et al., 1994). The hydrogen bond between Lys<sup>19</sup> O' and Gly<sup>22</sup> H<sup>N</sup> expected in a Schellman motif is not present in our structures. Instead, we see Gly<sup>22</sup> H<sup>N</sup> in a position to make another hydrogen bond extending an  $\alpha$ -helix. The experimental constraints found for Gly<sup>22</sup> H<sup>N</sup> are relatively unrestrictive and the final conformation of this residue results at least partially from the energy minimization. Among four toxins shown in Figure 8, there are 6–9 residues separating cysteine 18 (numbering of AgTx2) and invariable Gly<sup>26</sup>. Only the helix of the P05-NH<sub>2</sub> toxin analog, with six residues between the conserved cysteine and glycine, ends with an  $\alpha_L$  motif (Aurora et al., 1994). The helices of three remaining toxins end in a more or less distorted Schellman motif.

The positive value of  $\phi$  torsion angle of Arg<sup>31</sup> in the type II reverse turn is strikingly similar to the positive  $\phi$  torsion angle of Phe<sup>44</sup> of Stv3 involved in its type III' reverse turn. Such a conformation allows the formation of the hydrogen bond between Cys<sup>8</sup> H<sup>N</sup> and Arg<sup>31</sup> O' in AgTx2, and Cys<sup>16</sup> H<sup>N</sup> and Phe<sup>44</sup> O' in Stv3, respectively. The turn conformation is also very similar in the P05-NH<sub>2</sub> scorpion toxin analog, but the poor definition of Cys<sup>3</sup> does not permit a more detailed comparison.

The length of disulfide bonds in AgTx2 follows the trend observed in other scorpion toxins. The first disulfide (Cys<sup>8</sup>–Cys<sup>28</sup>) is consistently longer, with about 6.5 Å separation between C<sup>α</sup> atoms of the connected residues. The other two disulfide bonds separate their respective C<sup>α</sup> atoms by about 5.5 Å. The isomerization of the disulfide bond handedness was observed in the high-resolution X-ray structures of Stv3 (Zhao et al., 1992). It was also postulated for the P05-NH<sub>2</sub> scorpion toxin analogue (Meunier et al., 1993). We did not observe any additional resonances that could indicate such a situation for AgTx2. However, the Cys<sup>18</sup>–Cys<sup>35</sup> disulfide bond in the final calculated structures does show two isomers.

The tertiary structure of AgTx2 closely resembles structures of related scorpion toxins: ChTx, IbTx, and MgTx. All of them were determined by solution NMR techniques. Among these toxins, the structure of AgTx2 is based on the largest number of distance and angle constraints. Correspondingly, the ensemble of calculated structures shows the smallest RMSDs of the back-

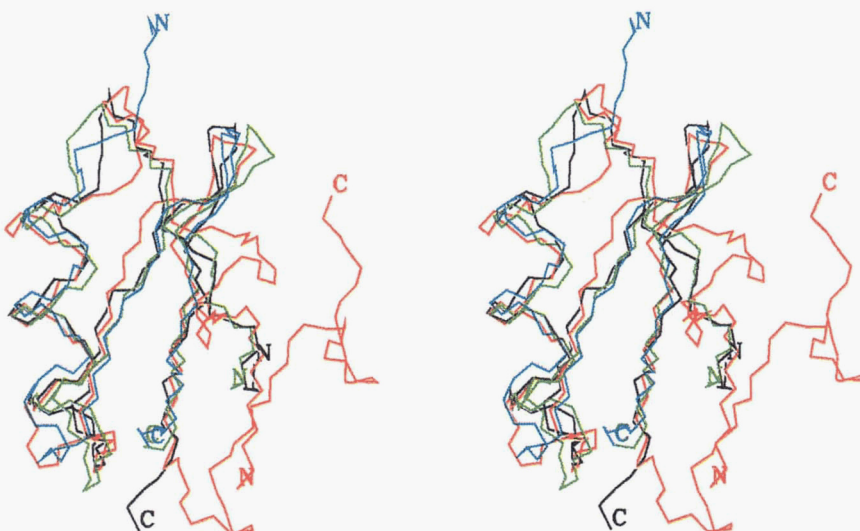


**Fig. 7.** Stereo diagram of superimposed backbone structures of scorpion toxins. The N- and C-termini are indicated. Black, AgTx2; red, Stv3; green, ChTx; blue, PO5-NH<sub>2</sub> scorpion toxin analogue.

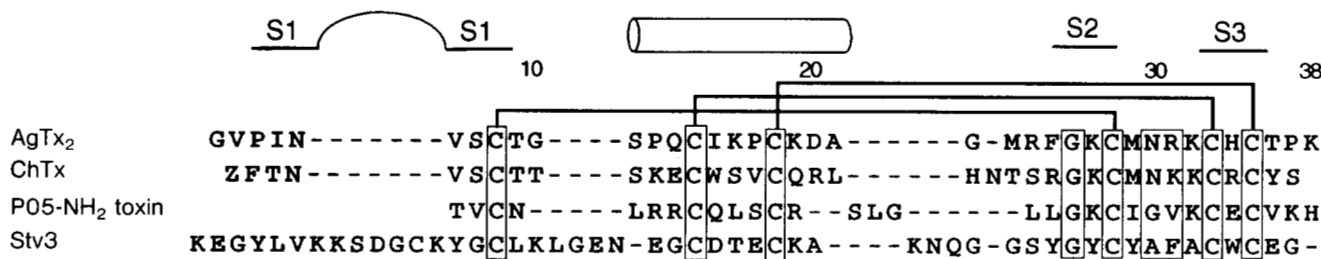


**Fig. 8.** Alignment of sequences of four scorpion toxins shown in Figure 7. Alignment was based on spatial correspondence of the N, C<sup>α</sup>, C' backbone atoms in various toxins. Secondary structure elements common in all toxins are indicated above the sequences. Residue numbering is for AgTx2. Disulfide bonds, the conserved Gly<sup>26</sup>, and the conserved β-turn centered around residues 30 and 31 are indicated with boxes.

bone and side chain atoms. The recently reported solution structure of MgTx is comparably well defined (Johnson et al., 1994). The superposition of backbone atoms of equivalent residues (see Table 5) shows that the backbone structure of AgTx2 is most similar to the structure of Stv3.

KTx has a sequence almost 90% identical to AgTx2. The recently determined <sup>1</sup>H assignments and the solution structure of KTx (Fernandez et al., 1994) are remarkably different from the results we obtained for AgTx2. The proposed structure of KTx has the N-terminal strand of the β-sheet positioned on the opposite side of the S2-S3 hairpin plane. Considering the high degree of sequence homology, this structural difference is rather unlikely, and a further analysis of the KTx structure may be required.

The binding affinity and specificity of AgTx2 to the *Shaker* K<sup>+</sup> channel crucially depends on three residues Arg<sup>24</sup>, Lys<sup>27</sup>, and Arg<sup>31</sup> (Fig. 9; see Kinemage 1) (Hidalgo & MacKinnon, 1995). Two of them (24 and 31) are positioned at the two opposite ends of the molecule along its long axis. Lys<sup>27</sup> is located almost exactly halfway between them. Arg<sup>24</sup> interacts closely with Phe<sup>25</sup> and with the C-terminal Lys<sup>38</sup>. As a consequence, its side-chain conformation is well defined by many NOE constraints. On the other hand, the conformation of the side chain of Lys<sup>27</sup> is not restricted by any constraints. Similarly, the side chain of Arg<sup>31</sup> is not constrained beyond the C<sup>γ</sup> atom. The narrow linewidths of Lys<sup>27</sup> and Arg<sup>31</sup> side chain protons indicate that they are probably highly mobile in solution. One can speculate that the mobility of these side chains facilitates the forma-

tion of the initial complex between the toxin and the K<sup>+</sup> channel. It remains to be seen whether these side chains adopt well-defined conformations when bound to the channel.

ChTx inhibits the *Shaker* K<sup>+</sup> channels 300-fold weaker than AgTx2. The peptide backbone of AgTx2 superimposes well with that of ChTx throughout much of its length. However, a significant difference in the structures of AgTx2 and ChTx occurs where the C3-C4 segment forms a loop connecting the C-terminal end of the α-helix to the β-sheet. The Arg<sup>19</sup> of ChTx is equivalent to Asp<sup>20</sup> of AgTx2. Following this position in AgTx2 are residues with small side chains (Ala<sup>21</sup> and Gly<sup>22</sup>). Structurally corresponding residues in ChTx are much bulkier (Leu<sup>20</sup> and His<sup>21</sup>). Additionally, Asn<sup>22</sup> of ChTx is deleted from the sequence of AgTx2. On the other hand, in AgTx2, the aromatic side chain of Phe<sup>25</sup> interacts with the side chain of Arg<sup>24</sup>, restricting the mobility of the latter. As a result, AgTx2 contains a well-defined positively charged residue (Arg<sup>24</sup>) at a very specific location, near the edge of the molecule, but still below the plane of the β-sheet. Arg<sup>19</sup> and Arg<sup>25</sup> of ChTx even though relatively close neighbors are not nearly as conformationally restricted, and they are also not positioned that close to the edge of the β-sheet. These findings provide a structural basis for the very different interactions of AgTx2 and ChTx with Asp<sup>431</sup> near the pore entryway of the *Shaker* K<sup>+</sup> channel.

Our current model of the agitoxin 2 binding to the *Shaker* K<sup>+</sup> channel is schematically depicted in Figure 10. The negatively charged Asp<sup>431</sup> of the *Shaker* K<sup>+</sup> channel homotetramer (MacKinnon, 1991) interacts with Arg<sup>24</sup> and Arg<sup>31</sup> of agitoxin 2. Lys<sup>27</sup>

**Table 5.** RMSDs in Å among the polypeptide backbones atoms (N, C<sup>α</sup>, C') of selected scorpion toxin structures<sup>a</sup>

AgTx2	2-21, 23-37 3-22, 23-37	5-13, 17-29 11-19, 24-36	3-5, 14-18, 25-31, 35-50 2-4, 6-10, 14-20, 22-37
1.10	ChTx	5-13, 17-29 10-18, 24-36	3-5, 14-18, 25-31, 35-50 1-3, 5-9, 13-19, 22-37
1.23	1.37	P05-NH <sub>2</sub> scorpion toxin analog	25-30, 37-49 8-13, 17-29
0.88	1.48	0.82	Stv3

<sup>a</sup> Names of the toxins are given in the diagonal cells; RMSDs between the toxins are shown in the lower triangle. The cells in the upper triangle identify the polypeptide segments used for the superpositions; the top and bottom lines in those cells list the segments of the toxins in the same columns and rows, respectively.

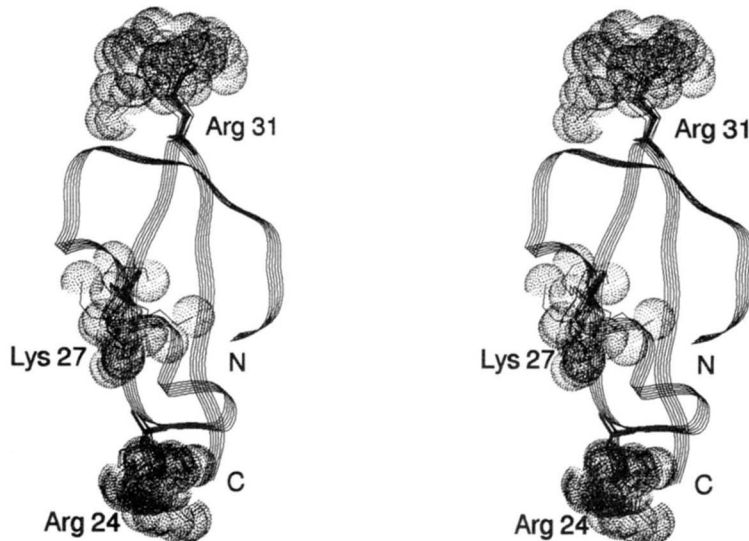


**Fig. 9.** Stereo diagram of the agitoxin structure. Side chains of residues Arg<sup>24</sup>, Lys<sup>27</sup>, and Arg<sup>31</sup> for 17 structures are shown. The N<sup>η</sup> atoms of arginines and N<sup>c</sup> atoms of lysines are indicated by dotted van der Waals surfaces.

is positioned over the center of the channel. The exact conformation of the side chain of Lys<sup>27</sup> in the bound form is not known. However, the maximum radius of the area covered by the side chain of Lys<sup>27</sup>, allowing for all possible rotamers, is about 5 Å.

#### Materials and methods

##### Materials

Trypsin used for the preparations was purchased from Worthington Biochemical Corporation (Freehold, New Jersey). The <sup>15</sup>NH<sub>4</sub>Cl (99% <sup>15</sup>N) was obtained from Isotec (Miamisburg, Ohio). *Escherichia coli* strain DH5a was used for plasmid propagation and strain BL21(DE3) was used for expression of the fusion protein. The plasmid pCSP105 was a gift from C. Miller (Brandeis University). The AgTx2 plasmid was constructed from pCSP105 as previously described (Park et al., 1991; Garcia et al., 1994).

#### Expression and purification of AgTx2

*E. coli* strain BL21 harboring the AgTx2 plasmid were cultured in rich media (LB medium) and induced with isopropyl 1-thio-β-D-galactopyranoside. Purification of the toxin was carried out as described (Garcia et al., 1994), except that 5 µg of trypsin per milligram of fusion protein was added to cleave AgTx2 from the fusion protein. AgTx2 was purified from the cleavage mixture by SP Sephadex followed by C<sub>8</sub> reversed-phase HPLC using a linear gradient of acetonitrile (0–50%, 30 min). Individuals peaks were collected, lyophilized, and stored at –20 °C. The final yield was 2 mg of AgTx2 per liter of culture. The composition of the purified material was verified by mass spectrometry and amino acid analysis.

#### Expression and purification of <sup>15</sup>N-AgTx2

The synthesis was the same as described above, with the following modifications. *E. coli* strain BL21 carrying the AgTx2 plasmid was cultured in minimal media. The minimal media contained (in g/L) Na<sub>2</sub>HPO<sub>4</sub>·7H<sub>2</sub>O, 12.8; KH<sub>2</sub>PO<sub>4</sub>, 3.0; NaCl, 0.5; <sup>15</sup>NH<sub>4</sub>Cl, 1.0; (in mM) MgSO<sub>4</sub>, 2.0; CaCl<sub>2</sub>, 0.1; and 0.2% glucose. The final yield was 0.7 mg of <sup>15</sup>N-AgTx2 per liter of culture.

#### NMR samples preparation

Protein samples used for homonuclear NMR experiments were about 1 mM in either 90% H<sub>2</sub>O/10% D<sub>2</sub>O or 100% D<sub>2</sub>O, at pH 4.5. Uniformly isotope enriched samples were 300 µM in 90% H<sub>2</sub>O/10% D<sub>2</sub>O at the same pH (uncorrected for the isotope effect).

#### NMR spectroscopy

Sequence-specific resonance assignments were obtained by standard homonuclear 2D NMR experiments (Wagner & Wüthrich, 1982; Wüthrich, 1986). All NMR experiments were carried out

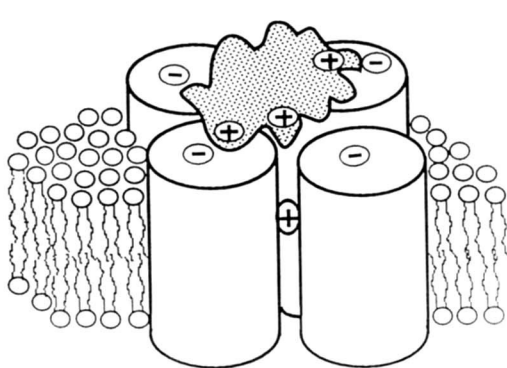


**Fig. 10.** Schematic diagram of the AgTx2 blocking the Shaker K<sup>+</sup> channel. Pluses and minuses indicate the positively and negatively charged residues of the AgTx2 (Arg<sup>24</sup>, Lys<sup>27</sup>, and Arg<sup>31</sup>) and channel (Asp<sup>431</sup>).

on Bruker AMX500 and AMX600 spectrometers at 25 °C. The solvent signal was suppressed by low-level presaturation during the relaxation delay. Sweep widths were 12,500 Hz (2,048 complex data points) in acquisition dimension, and 6,250 Hz (256 complex points) in indirect dimension. Spectra were referenced to water signal (4.80 ppm). The NOESY mixing time used was 250 ms and the DIPSI mixing time in TOCSY experiments was 80 ms. Data were processed using the Felix software (Biosym Technologies, San Diego, California). The real matrix sizes of the processed spectra were 8,192 by 4,096 points.

### Conformational constraints

Distance constraints for the structure calculations were obtained from two NOESY spectra recorded in 90% H<sub>2</sub>O/10% D<sub>2</sub>O and 100% D<sub>2</sub>O, respectively. Cross peak intensities were estimated by counting contour levels on plots drawn with log<sub>1.4</sub> scale. The strongest observed H<sub>i</sub><sup>α</sup>-H<sub>i+1</sub><sup>N</sup> cross peaks were assumed to correspond to 2.8 Å. Coupling constants <sup>3</sup>J(H<sup>α</sup>, H<sup>N</sup>) were obtained from measurements of the ratios of cross peak to diagonal peak volumes in a 3D HNHA experiment (Vuister & Bax, 1993). Torsion angle restraints were generated from the coupling constants using built-in routines of the NMRchitect module in the Biosym molecular modeling software package (version 2.30; Biosym Technologies, San Diego, California). The Karplus curve parameters were A = 6.51, B = -1.76, C = 1.60 (Vuister & Bax, 1993). The allowed range of restricted torsion angles was at least ±30°. Information on the H<sup>N</sup>-H<sup>β</sup> vicinal coupling constant was obtained from a qualitative interpretation of an HNHB experiment as described previously (Archer et al., 1991; Mad-sen et al., 1993). This was combined with qualitative information on H<sup>α</sup>-H<sup>β</sup> coupling constants from a DQF-COSY spectrum to derive stereospecific assignments of the β-methylene protons and χ<sup>1</sup> angle restraints (Wagner, 1990). Hydrogen bond constraints were included based on indicative NOEs observed for antiparallel β-sheet and α-helix (Wüthrich, 1986). The slow rate of exchange of the amide proton, as measured in DQF-COSY spectra recorded 24 h after dissolving the protein in 100% D<sub>2</sub>O was also a criterion for a hydrogen bond donor.

### Structure calculations

Structural models were calculated using distance geometry routines (Havel, 1992) in the NMRchitect module of the Biosym molecular modeling software package, as described previously (Withka et al., 1993). Five hundred structures were embedded using the experimental constraints and optimized by simulated annealing. The 50 structures with the lowest residual violations (target function value below 0.1) were then subjected to restrained energy minimization using the Discover module (version 2.95) of the Biosym molecular modeling software package. The best 17 structures presented in this report were selected on the basis of the total energy and maximum residual distance violations. The maximum allowed potential energy and distance violation were arbitrarily chosen at 380.0 kcal (within 10% of the lowest energy structure) and 0.3 Å, respectively. The constraint forcing potentials for minimized structures were below 12.0 kcal, as reported by the Discover program (Biosym). The solvent accessibility with the water probe size of 1.4 Å was calculated using routines of the InsightII program (Biosym). The

coordinates and the list of the constraints have been deposited with the Brookhaven Protein Data Bank (access code 1AGT).

### Supplementary material in Electronic Appendix

The complete list of conformational constraints is available in the Electronic Appendix (SUPLEMNT directory, file Krezel\_NMR).

### Acknowledgments

This work was supported by NIH grants GM47467 to G.W. and GM43949 to R.M. We thank Joanne M. Williamson for advice on isotope labeling and Dr. Peter Schmieder for the advice on <sup>15</sup>N-separated experiments. Acquisition of computers used in this work was supported by the Keck Foundation.

### References

- Anil-Kumar, Ernst RR, Wüthrich K. 1980. A two-dimensional nuclear Overhauser enhancement (2D NOE) experiment for the elucidation of complete proton-proton cross-relaxation networks in biological macromolecules. *Biochem Biophys Res Commun* 95:1-6.
- Archer SJ, Ikura M, Torchia DA, Bax A. 1991. An alternative 3D NMR technique for correlating backbone <sup>15</sup>N with side chain H<sup>β</sup> resonances in larger proteins. *J Magn Reson* 95:636-641.
- Aurora R, Srinivasan R, Rose GD. 1994. Rules for α-helix termination by glycine. *Science* 264:1126-1130.
- Bodenhausen G, Ruben DJ. 1980. Natural abundance nitrogen-15 NMR by enhanced heteronuclear spectroscopy. *Chem Phys Lett* 69:185-189.
- Bonmatin JM, Bonnat JC, Gallet X, Vovelle F, Ptak M, Reichhart JM, Hoffmann JA, Keppi E, Legrain M, Achstetter T. 1992. Two-dimensional <sup>1</sup>H NMR study of recombinant insect defensin A in water: Resonance assignments, secondary structure and global folding. *J Biomol NMR* 2:235-256.
- Bontems F, Gilquin B, Roumestand C, Menez A, Toma F. 1992. Analysis of side-chain organization on a refined model of charybdotoxin: Structural and functional implications. *Biochemistry* 31:7756-7764.
- Bontems F, Roumestand C, Boyot P, Gilquin B, Doljansky Y, Menez A, Toma F. 1991a. Three-dimensional structure of natural charybdotoxin in aqueous solution by <sup>1</sup>H-NMR. Charybdotoxin possesses a structural motif found in other scorpion toxins. *Eur J Biochem* 196:19-28.
- Bontems F, Roumestand C, Gilquin B, Menez A, Toma F. 1991b. Refined structure of charybdotoxin: Common motifs in scorpion toxins and insect defensins. *Science* 254:1521-1523.
- Braunschweiler L, Ernst RR. 1983. Coherence transfer by isotropic mixing: Application to proton correlation spectroscopy. *J Magn Reson* 53:521-528.
- Fernandez I, Romi R, Szendeffi S, Martin-Eauclaire MF, Rochat H, Van Rietschoten J, Pons M, Giralt E. 1994. Kalitoxin (1-37) shows structural differences with related potassium channel blockers. *Biochemistry* 33:14256-14263.
- Garcia ML, Garcia-Calvo M, Hidalgo P, Lee A, MacKinnon R. 1994. Purification and characterization of three inhibitors of voltage-dependent K<sup>+</sup> channels from *Leiurus quinquestriatus* var. *hebraeus* venom. *Biochemistry* 33:6834-6839.
- Giangiacomo KM, Garcia ML, McManus OB. 1992. Mechanism of iberiotoxin block of the large-conductance calcium-activated potassium channel from bovine aortic smooth muscle. *Biochemistry* 31:6719-6727.
- Havel TF. 1991. An evaluation of computational strategies for use in the determination of protein structure from distance constraints obtained by nuclear magnetic resonance. *Prog Biophys Mol Biol* 56:43-78.
- Hidalgo P, MacKinnon R. 1995. Revealing the architecture of a K<sup>+</sup> channel pore through mutant cycles with a peptide inhibitor. *Science* 268:307-310.
- Hyberts SG, Goldberg MS, Havel TF, Wagner G. 1992. The solution structure of eglin c based on measurements of many NOEs and coupling constants and its comparison with X-ray structures. *Protein Sci* 1:736-751.
- IUPAC-IUB Commission on Biochemical Nomenclature. 1970. Abbreviations and symbols for the description of the conformation of polypeptide chains. *J Mol Biol* 52:1-17.
- Jeener J, Meier BH, Bachmann P, Ernst RR. 1979. Investigation of exchange processes by two-dimensional NMR spectroscopy. *J Chem Phys* 71:4546-4553.

- Johnson BA, Stevens SP, Williamson JM. 1994. Determination of the three-dimensional structure of margatoxin by  $^1\text{H}$ ,  $^{13}\text{C}$ ,  $^{15}\text{N}$  triple-resonance nuclear magnetic resonance spectroscopy. *Biochemistry* 33:15061–15070.
- Johnson BA, Sugg EE. 1992. Determination of the three-dimensional structure of iberiotoxin in solution by  $^1\text{H}$  nuclear magnetic resonance spectroscopy. *Biochemistry* 31:8151–8159.
- Kraulis PJ. 1991. MOLSCRIPT: A program to produce both detailed and schematic plots of protein structures. *J Appl Crystallogr* 24:946–950.
- Laskowski RA, MacArthur MW, Moss DS, Thornton JM. 1993. PROCHECK: A program to check the stereochemical quality of protein structures. *J Appl Crystallogr* 26:283–291.
- MacKinnon R. 1991. Determination of the subunit stoichiometry of a voltage-activated potassium channel. *Nature* 350:232–235.
- MacKinnon R, Miller C. 1988. Mechanism of charybdotoxin block of the high-conductance  $\text{Ca}^{2+}$ -activated  $\text{K}^+$  channel. *J Gen Physiol* 91:335–349.
- MacKinnon R, Miller C. 1989. Functional modification of a  $\text{Ca}^{2+}$ -activated  $\text{K}^+$  channel by trimethyloxonium. *Biochemistry* 28:8087–8092.
- Madsen JC, Sørensen OW, Sørensen P, Poulsen FM. 1993. Improved pulse sequences for measuring coupling constants in  $^{13}\text{C}$ ,  $^{15}\text{N}$ -labeled proteins. *J Biomol NMR* 3:239–244.
- Meunier S, Bernassau JM, Sabatier JM, Martin-Eauclaire MF, Van Riet-schoten J, Cambillau C, Darbon H. 1993. Solution Structure of PO5-NH<sub>2</sub>, a scorpion toxin analog with high affinity for the apamin-sensitive potassium channel. *Biochemistry* 32:11969–11976.
- Miller C. 1988. Competition for block of a  $\text{Ca}^{2+}$ -activated  $\text{K}^+$  channel by charybdotoxin and tetraethylammonium. *Neuron* 1:1003–1006.
- Miller C, Moczydowski E, Latorre R, Phillips M. 1985. Charybdotoxin, a protein inhibitor of single  $\text{Ca}^{2+}$ -activated channels from mammalian skeletal muscle. *Nature* 313:316–318.
- Park CS, Hausdorff SF, Miller C. 1991. Design, synthesis and functional expressions of a gene for charybdotoxin, a peptide blocker of  $\text{K}^+$  channels. *Proc Natl Acad Sci USA* 88:2046–2050.
- Piantini U, Sørensen OW, Ernst RR. 1982. Multiple quantum filters for elucidating NMR coupling networks. *J Am Chem Soc* 104:6800–6801.
- Ramachandran GN, Ramakrishnan C, Sasisekharan V. 1963. Stereochemistry of polypeptide chain configurations. *J Mol Biol* 7:95–99.
- Rance M, Sørensen OW, Bodenhausen G, Wagner G, Ernst RR, Wüthrich K. 1983. Improved spectral resolution in COSY  $^1\text{H}$  NMR spectra. *Biochem Biophys Res Commun* 117:479–485.
- Shaka AJ, Freeman R. 1983. Simplification of NMR spectra by filtration through multiple-quantum coherence. *J Magn Reson* 51:169–173.
- Stampe P, Kolmakova-Partensky L, Miller C. 1994. Intimations of  $\text{K}^+$  channel structure from a complete functional map of the molecular surface of charybdotoxin. *Biochemistry* 33:443–450.
- Vuister GW, Bax A. 1993. Quantitative *J* correlation: A new approach for measuring homonuclear three-bond  $J(\text{H}^1\text{N}^1\text{H}^\alpha)$  coupling constants in  $^{15}\text{N}$ -enriched proteins. *J Am Chem Soc* 115:7772–7777.
- Wagner G. 1990. NMR investigations of protein structure. *Prog Nucl Magn Reson Spectrosc* 22:101–139.
- Wagner G, Wüthrich K. 1982. Sequential resonance assignments in protein  $^1\text{H}$  nuclear magnetic resonance spectra. Basic pancreatic trypsin inhibitor. *J Mol Biol* 155:347–366.
- Withka JM, Wyss DF, Wagner G, Arulanandam ARN, Reinherz EL, Recny MA. 1993. Structure of the glycosylated adhesion domain of human T lymphocyte glycoprotein CD2. *Structure* 1:69–81.
- Wüthrich K. 1986. *NMR of proteins and nucleic acids*. New York: John Wiley & Sons.
- Zhao B, Carson M, Ealick SE, Bugg CE. 1992. Structure of scorpion toxin variant-3 at 1.2 Å resolution. *J Mol Biol* 227:239–252.